scientific reports

OPEN

Importance of d_{xy} orbital and electron correlation in iron-based superconductors revealed by phase diagram for 1111-system

Tsuyoshi Kawashima[1], Shigeki Miyasaka[1]✉, Hirokazu Tsuji[1], Takahiro Yamamoto[1], Masahiro Uekubo[1], Akira Takemori[1], Kwing To Lai[1,2] & Setsuko Tajima[1]

The structural flexibility at three substitution sites in LaFeAsO enabled investigation of the relation between superconductivity and structural parameters over a wide range of crystal compositions. Substitutions of Nd for La, Sb or P for As, and F or H for O were performed. All these substitutions modify the local structural parameters, while the F/H-substitution also changes band filling. It was found that the superconducting transition temperature T_c is strongly affected by the pnictogen height h_{Pn} from the Fe-plane that controls the electron correlation strength and the size of the d_{xy} hole Fermi surface (FS). With increasing h_{Pn}, weak coupling BCS superconductivity switches to the strong coupling non-BCS one where electron correlations and the d_{xy} hole FS may be important.

Identifying the mechanism of high-temperature superconductivity has been a challenging task in solid state physics. For iron pnictide superconductors[1,2], more than 10 years' effort has been devoted to clarifying the superconductivity mechanism. However, the essential problem of a pairing glue is still under debate. In many iron-based superconductors, the superconducting phase is observed near the quantum critical point of magnetic order[3] and/or nematic order[4]. This suggests a spin or orbital fluctuation as pairing glue. On the other hand, the Fermi surface (FS) topology of iron-based superconductors has a strong material dependence[5–15], which causes difficulties in clarifying the superconducting mechanism from the viewpoints of FS nesting related with the spin or orbital fluctuation. Instead of FS nesting approach, a lot of other theoretical models have been proposed to explain their superconducting mechanism[16–23]. One of these proposals emphasizes strong electron correlation near the Mott insulator regime[16–18], rather than a magnetic or orbital fluctuation in the weak-coupling regime.

Experimentally, it is well known that there is a correlation between the superconducting transition temperature (T_c) and local crystal structure parameters, such as the pnictogen height (h_{Pn}) from the Fe-layer, and the As–Fe–As bond angle (α). First, Lee et al. demonstrated that T_c reaches a maximum when α is close to 109.47°, corresponding to the value for a regular FeAs$_4$ tetrahedron[24]. A similar correlation was found between T_c and h_{Pn}[25]. Here the maximum T_c was observed at $h_{Pn} \sim 1.38$ Å. The main questions are: which physical parameters are controlled by these structural parameters, and how do they contribute to superconductivity?

According to theoretical calculations, the d_{xy} hole FS around (π, π) in the unfolded Brillouin zone expands with increasing h_{Pn}[26]. However, it is not obvious how this electronic change controls superconductivity. In fact, in the LaFeAsO (La-1111) system, T_c does not vary monotonically with changes in lattice parameters[27–29]. Our previous studies have revealed that there are three superconducting phases in LaFe(As,P)(O,F/H), depending on the compositions[29]. Although bosonic fluctuation via FS nesting was discussed as the most plausible pairing mechanism, the high T_c in the third superconducting phase (SC3) could not be explained using the same scenario, because the nesting condition is very bad. Here it is unclear which structural parameter switches the mechanism, and how. As an alternative to the FS nesting based weak-coupling model, it is worth examining other scenario based on strong electron correlation near the d^5 Mott insulator regime[16,18]. Here it is unclear which structural parameter switches the mechanism, and how.

[1]Department of Physics, Osaka University, Toyonaka, Osaka, 560-0043, Japan. [2]Department of Physics, The Chinese University of Hong Kong, Shatin, Hong Kong, China. ✉email: miyasaka@phys.sci.osaka-u.ac.jp
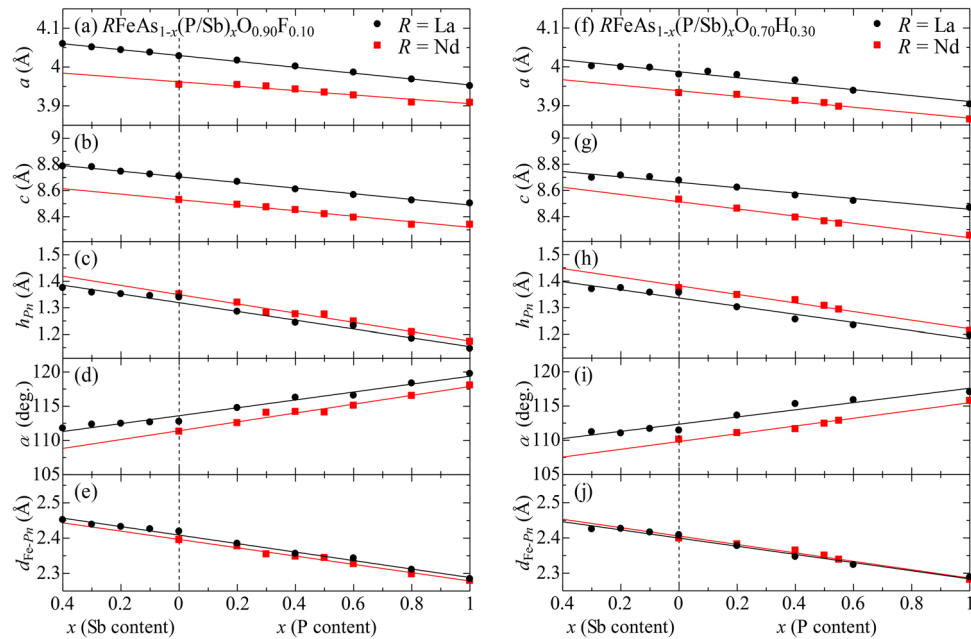
Figure 1. x-dependence of structural parameters for (**a–e**) RFeAs$_{1-x}$(P/Sb)$_x$O$_{0.90}$F$_{0.10}$ and (**f–j**) RFeAs$_{1-x}$(P/Sb)$_x$O$_{0.70}$H$_{0.30}$ (R = La and Nd). (**a, f**) Lattice constant a. (**b, g**) Lattice constant c. (**c, h**) Pnictogen height from the Fe plane, h_{Pn}. (**d, i**) Pn–Fe–Pn bond angle α. (**e, j**) Fe–Pn bond length d_{Fe-Pn}. Structural parameters for other compositions are shown in Supplementary Information (Fig. S1).

In this study, we extended our previous work on LaFe(As,P)(O,F/H)[29] by covering a wider range of structural parameters through three site substitutions (Nd for La, Sb or P for As, and F or H for O). All these substitutions modify the local structural parameters, while the F/H-substitution also changes band filling. (In other iron-based superconductors, AFe$_2$As$_2$ systems (A = Ba, Sr, and Ca), the phase diagrams and T_c have been investigated from the viewpoints of local structural parameters and carrier doping level[30].) Precise measurements of structural parameters and resistivity for all samples revealed that the d_{xy} hole FS is crucially important in a wide doping range for the high h_{Pn} compounds. Although there are apparently three SC phases, two of them (SC1 and SC3) turn out to be of the same origin. It is likely that with increasing h_{Pn} electron correlation becomes strong, which switches the FS nesting based weak coupling superconductivity (SC2) to other type of superconductivity such as the one derived from orbital-selective Mott systems (SC1/SC3). T-linear resistivity was commonly observed near the T_c-maximum composition in each phase.

Results

First, we present structural data for several typical compositions. (Data for all remaining compositions are provided in the "Supplementary Information".) Figure 1a,b,f,g show the lattice constants a and c as functions of P/Sb content (x) for RFeAs$_{1-x}$(P/Sb)$_x$O$_{1-y}$(F/H)$_y$ with y = 0.1 and 0.3 (R = La and Nd). Part of the dataset is taken from our previous papers[27–29]. The P/Sb contents (x) were determined by energy-dispersive X-ray spectroscopy (EDX), while the F/H compositions (y) are nominal values. Here we see that the lattice constants vary linearly with x according to Vegard's law, demonstrating the successful substitution of P or Sb for As. The result indicates that P-substitution has the effect of lattice compression, while the Sb-substitution has the opposite effect. More detailed structural parameters, such as the pnictogen (Pn) height from the Fe-plane (h_{Pn}), the Pn–Fe–Pn bond angle (α) and the Fe–Pn bond distance (d_{Fe-Pn}) are presented in Fig. 1c–e,h–j. These parameters also vary linearly with x. With increasing Sb-content, thereby expanding the lattice, h_{Pn} and d_{Fe-Pn} increase, while α decreases. In Nd-systems, although the lattice constants are smaller, h_{Pn} is larger and α is smaller than in the La-systems. As will be discussed later, among all these parameters, h_{Pn} and/or α plays the most crucial role in determining the electronic state. From the present results, we find that the common primary effect of P/As(Sb), O/F(H) and La/Nd substitutions is to increase h_{Pn}.

To observe the change in carrier interaction, we measured the temperature (T) dependence of resistivity (ρ). In Fig. 2, the T-dependence of $\rho - \rho_0$ is plotted on a log-scale, where ρ_0 is residual resistivity. In all systems, with increasing P-content x, $\rho - \rho_0$ changed from non-Fermi liquid-like T-linear behavior to T^2-behavior. This implies that As-rich compositions are in the strong interaction regime, while with increasing P-content, the interaction is weakened, and the system becomes a Fermi liquid. (It should be noted that, although the T^2-behavior of resistivity could be induced by disorders in the strong coupling superconductors[31], residual resistivity in the present compounds systematically decreases with x and reaches the lowest value at x = 1.0 where $\rho \sim T^2$. This means that T^2-behavior of resistivity is not due to disorder in the present case.) Accordingly, as seen in the insets, T_c decreases with increasing P-content.
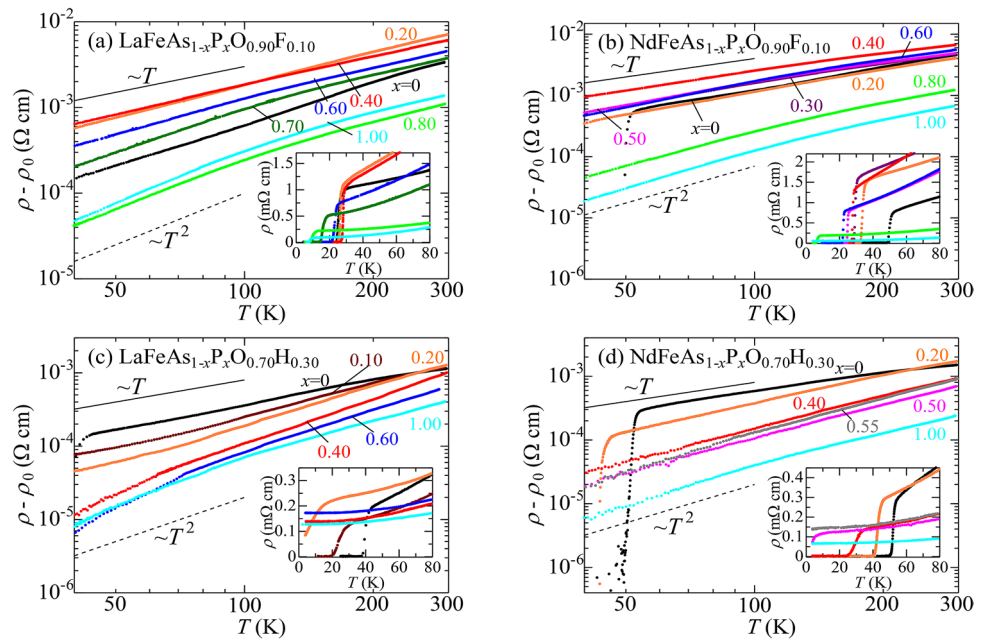
Figure 2. Temperature (T-) dependence of $\rho - \rho_0$ for RFeAs$_{1-x}$P$_x$O$_{0.90}$F$_{0.10}$ and RFeAs$_{1-x}$P$_x$O$_{0.70}$H$_{0.30}$ (R = La and Nd), where ρ_0 is residual resistivity. (**a**) LaFeAs$_{1-x}$P$_x$O$_{0.90}$F$_{0.10}$. (**b**) NdFeAs$_{1-x}$P$_x$O$_{0.90}$F$_{0.10}$. (**c**) LaFeAs$_{1-x}$P$_x$O$_{0.70}$H$_{0.30}$. (**d**) NdFeAs$_{1-x}$P$_x$O$_{0.70}$H$_{0.30}$. Insets of (**a**–**d**) show T-dependence of resistivity ρ at low temperatures. T-dependence of ρ for other compositions are shown in Supplementary Information (Figs. S2 and S3).
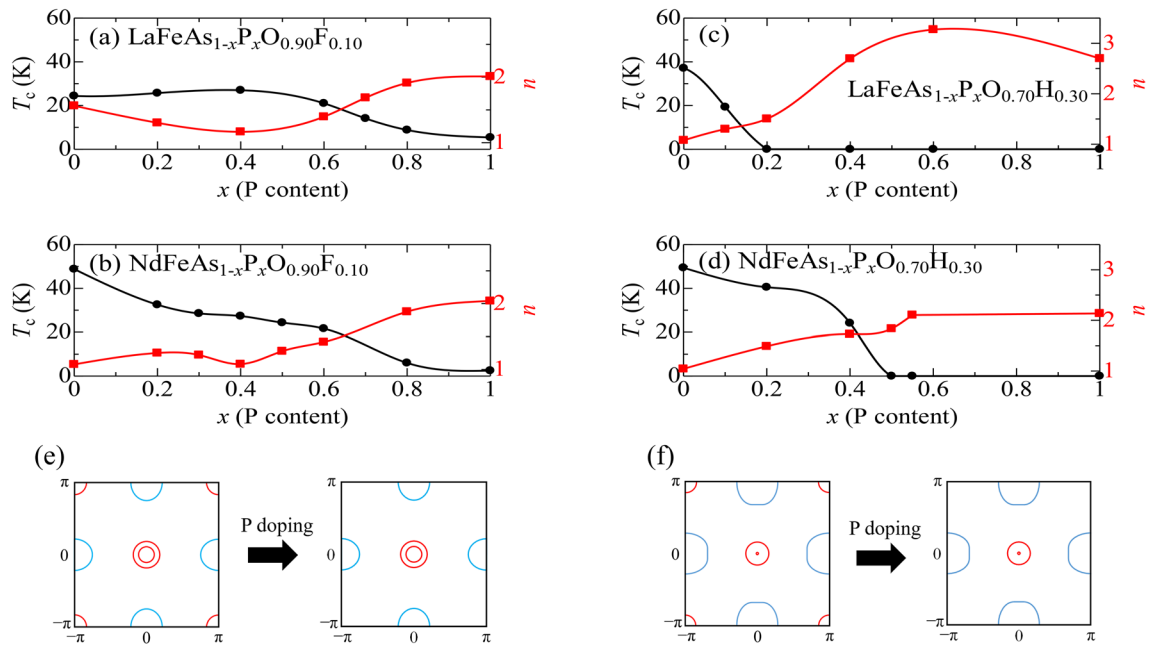

Figure 3. P concentration x-dependence of T_c (black circles) and n in $\rho(T) = \rho_0 + AT^n$ (red squares), and schematic Fermi surfaces, for $y = 0.1$ and 0.3. (**a**) LaFeAs$_{1-x}$P$_x$O$_{0.90}$F$_{0.10}$. (**b**) NdFeAs$_{1-x}$P$_x$O$_{0.90}$F$_{0.10}$. (**c**) LaFeAs$_{1-x}$P$_x$O$_{0.70}$H$_{0.30}$. (**d**) NdFeAs$_{1-x}$P$_x$O$_{0.70}$H$_{0.30}$. Solid lines are visual guides. (**e**, **f**) Schematic Fermi surfaces. Solid red and blue lines indicate hole and electron Fermi surfaces, respectively.

In Fig. 3, we plot T_c and the power n in $\rho(T) = \rho_0 + AT^n$ for all the P-doped samples in Fig. 2. Figure 3a,b show the results for $y = 0.1$. In both La- and Nd-systems, at P100% composition ($x = 1.0$), T_c is very low (about 5 K) and $n \sim 2$. With decreasing x, T_c gradually increases, while the power n monotonically decreases towards unity. This clear correlation between T_c and n demonstrates that the key interaction for superconductivity is strengthened with decreasing x, as we have previously reported[27–29]. When x decreases below $x = 0.4$, T_c increases further in the Nd-system, while it is almost unchanged in the La-system. Our previous studies demonstrated
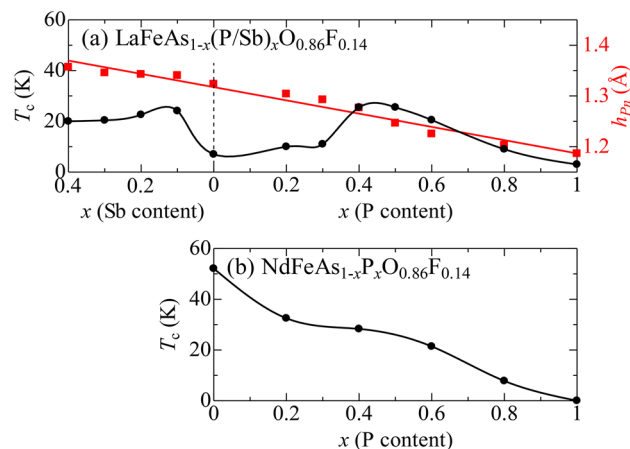
Figure 4. P(Sb) concentration x-dependence of T_c (black circles) for (**a**) $LaFeAs_{1-x}(P/Sb)_xO_{0.86}F_{0.14}$ and (**b**) $NdFeAs_{1-x}P_xO_{0.86}F_{0.14}$. The x-dependence of h_{Pn} (red squares) for $LaFeAs_{1-x}(P/Sb)_xO_{0.86}F_{0.14}$ is also shown in the (**a**). Solid lines are visual guides.

that there is a critical change in the electronic state at around $x = 0.4$. This was evidenced not only by transport properties such as resistivity and Hall coefficient, but also by direct observation of the band structural change through the angle-resolved photoemission experiment[13]. We distinguish these two superconducting regions, naming the As-rich region "SC1" and the P-rich region "SC2".

According to the theoretical calculations by Kuroki et al.[26], when h_{Pn} increases, the d_{xy} hole FS around (π, π) becomes larger. Therefore, when h_{Pn} decreases with x, as indicated in Fig. 1, the d_{xy} hole FS is expected to shrink and eventually disappear as illustrated in Fig. 3e. We believe this Fermi surface change drives the phase change from SC2 to SC1. The latter can be defined as the phase in which the d_{xy} hole FS contributes to superconductivity, while this is not expected in SC2. (Recently we observed d_{xy} band in $NdFeAs_{1-x}P_xO_{0.9}F_{0.1}$ by angle-resolved photoemission spectroscopy. It was experimentally confirmed that the d_{xy} band approaches the Fermi level at $x < 0.2$, forming an incipient band[32].)

For heavy electron-doping ($y = 0.3$), the n-value is much larger than one at $x = 1.0$, while it rapidly decreases when approaching $x = 0$. (See Fig. 3c,d.) At $x = 0$ where the high T_c of over 40 K is measured, n is close to 1, namely T-linear resistivity is observed. It is a common feature in the iron-based superconductors that while the P-rich compound is a weakly-interacting (Fermi-liquid like) system, the interaction becomes stronger with increasing As-content, which induces superconductivity and increases T_c. A significant difference from the lightly-doped case ($y = 0.1$) is that superconductivity disappears with P-substitution. As depicted in Fig. 3f, we expect that, with heavy electron doping, the electron FS becomes much larger than the hole FS at the zone center. This imbalance of hole- and electron-FS must prevent FS nesting-derived superconductivity in the P-rich compositions. Therefore, superconductivity in the P-rich compounds can be understood within the FS nesting scenario over a wide doping (y) range.

Since the d_{xy} hole FS at the zone corners shrinks and eventually disappears with increasing P-doping level x[33], we conclude that the d_{xy} orbital is crucially important for superconductivity for heavily electron doping. In the Nd-system, T_c remains high up to a larger x-value than in the La-system. This can be attributed to the larger d_{xy} hole FS due to the higher h_{Pn} in the Nd-system compared to the La-system.

We distinguish this heavily electron-doped region from the lightly doped region (SC1) by labelling it SC3, because the T_c is strongly suppressed in the intermediate range of y in the La-system. However, in the Nd-system, there is no such T_c suppression, and high T_c is maintained over a wide y-range. Considering that the difference between the La- and Nd-systems is caused by the greater pnictogen height (h_{Pn}), we enlarged h_{Pn} by Sb substitution for As in the La-system. An interesting example at $y = 0.14$ is shown in Fig. 4. In the Nd-system (Fig. 4b), the x-dependence of T_c at this doping level is qualitatively the same as that for $y = 0.10$. However, in the La-system (Fig. 4a), T_c is strongly depressed near $x = 0$, while it recovers with increasing Sb-content, probably because of the enlargement of the d_{xy} FS via the increase in h_{Pn}. This suggests that SC1 and SC3 have the same origin.

Discussion

Figure 5a,b are contour plots illustrating how T_c changes with x and y for the La- and Nd-systems, respectively. In these phase diagrams, we distinguish three superconducting phases (SC1, SC2 and SC3), particularly in the La-system. Compared to the change from SC1 to SC2 with the disappearance of the d_{xy} FS, the change from SC1 to SC3 is not clearly defined. In the La-system, although these two phases are separated at $x = 0$, when Sb is substituted, they merge with each other, as in the Nd-system, owing to the enlargement of the d_{xy} FS by the increase in h_{Pn}. We therefore think that the superconductivity mechanisms in phases SC1 and SC3 have the same origin. According to this scenario, the T_c suppression near $x = 0$ for the intermediate doping range ($0.14 < y < 0.25$) is not caused by the bad FS nesting condition, but by the loss of d_{xy} FS due to electron doping. The lost d_{xy} FS and suppressed T_c can be recovered by Sb substitution and/or electron doping.
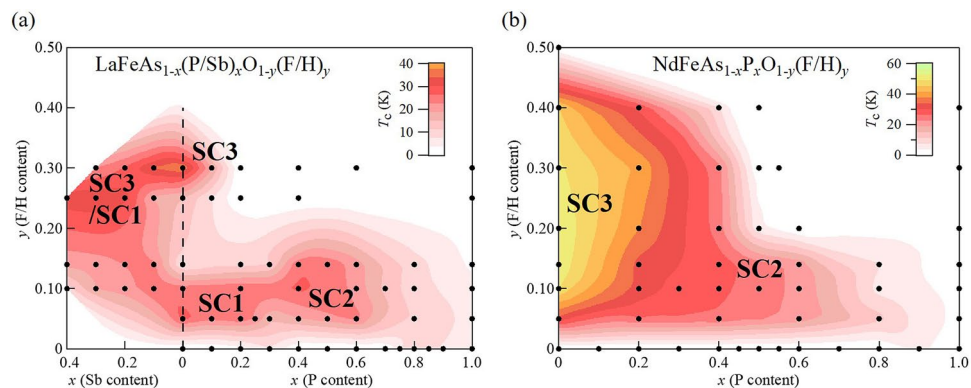
Figure 5. Schematic phase diagrams of (**a**) LaFeAs$_{1-x}$(P/Sb)$_x$O$_{1-y}$(F/H)$_y$ and (**b**) NdFeAs$_{1-x}$P$_x$O$_{1-y}$(F/H)$_y$. Dots represent the compositions examined in this study. Contour lines of T_c are drawn by extrapolation using the data of Figs. 3 and 4, "Supplementary materials", and previous results[27–29].
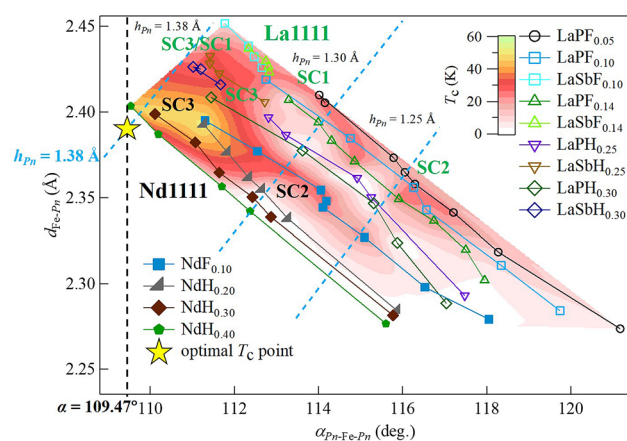

Figure 6. Contour plot of T_c for RFe(As,P/Sb)(O,F/H) systems (R = La and Nd). Symbols P, Sb, F, and H represent P, Sb, F, and H substitution, respectively. For each As/P(Sb)-substitution system, the SC phases lie on a straight line directed from lower right to upper left in the order SC2, SC1 and SC3. Blue broken lines indicate constant values of pnictogen height from the Fe plane, h_{Pn} = 1.25, 1.30, and 1.38 Å. The black broken line shows the constant value of the Pn–Fe–Pn bond angle $\alpha = 109.47°$. The yellow star indicates the optimal local crystal structure point corresponding to a regular tetrahedron of FePn_4.

To visualize the relation between the local structural parameters and T_c, Fig. 6 presents a contour plot of T_c in the α-$d_{\text{Fe}-Pn}$ plane. With electron doping, the bond angle (α) decreases. Moreover, T_c increases in the order of SC2, SC1 and SC3 as the structural parameters approach those for the regular tetrahedral structure.

This figure indicates that the local crystal structure strongly affects the T_c value in Fe-based superconductors. In SC3 phase where h_{Pn} is close to 1.38 Å, T_c is very high and insensitive to the band filling. Note that band filling should be another important parameter in weak coupling superconductivity where bosonic fluctuation via FS nesting acts as a pairing glue. In fact, in Fig. 6, the T_c suppression due to electron doping is visualized by the white bands extending from upper left to lower right. Therefore, in SC2 phase (P-rich compositions), the FS-nesting condition is crucially important, which supports a weak coupling regime[34–36]. However, in the large h_{Pn} region, there is no white area, namely, the FS-nesting condition does not affect T_c at all.

One of the theoretical scenarios is derived from strong electron correlations near the d^5 Mott insulator regime[16–18]. In this scenario, the total electron correlation is strong enough to induce antiferromagnetic order in LaFeAsO. Then, superconductivity is realized when the carriers are doped in this strongly-correlated parent compound. The electron correlation is enhanced with increasing h_{Pn}. Because h_{Pn} can be controlled by As(Sb)/P, and Nd/La substitutions, the T_c enhancement with these substitutions can be roughly interpreted as a result of increase in electron correlation. O/F(H) substitution has two effects, namely, carrier doping and increase in h_{Pn}. The former weakens the electron correlation, while the latter strengthens it. The apparent separation of SC1 and SC3 in the La-system (Fig. 5a) is a result of the competition of these two effects. In Fig. 6, we can see that the electron correlation is enhanced towards the optimal point. T-linear resistivity observed in SC3 (Fig. 3) is a common property of strongly-correlated superconductors. Another strength of this model is that the electron

correlation depends on the orbital, and the d_{xy} orbital plays a crucial role. This is consistent with the present results for SC1 and SC3.

There is another theoretical model for iron-based superconductors, shape resonance model[19–23], where T_c shows a clear enhancement around Lifshitz transition. In NdFeAs$_{1-x}$P$_x$(O,F), we observed the change of FS topology at Brillouin zone corner around $x = 0$–0.2, and that at zone center around $x = 0.2$–0.4 by angle-resolved photoemission spectroscopy measurement[13], which may correspond to Lifshitz transition. However, the T_c value changes gradually with x but does not show any abrupt change at a particular composition. So far, it is unclear whether this model can explain the observed complicated phase diagram in Fig. 5. Further experimental and theoretical studies are required to clarify that this model can be applied to the superconductivity mechanism of iron-based superconductors.

The evidence for the deviation from a weak coupling BCS regime can be seen in the so-called Uemura plot[37]. This famous plot demonstrates that many exotic superconductors, including cuprates, show a linear correlation between T_c and muon relaxation rate σ that is proportional to the superconducting carrier density. The important fact here is that these superconductors are characterized by low carrier density and high T_c, which suggests that the coupling interaction is extremely strong in these compounds, even beyond that of strong coupling superconductivity described by Eliashberg's theory. Namely, they are beyond BCS superconductors, and may be close to BCS-BEC crossover. Shortly after the discovery of Fe-based superconductors, σ was determined for several RFeAs(O,F) (R = La, Nd and Ce) compounds[38]. All the data points for the measured compounds lie on the Uemura line, indicating that these compounds are categorized as strong coupling exotic superconductors beyond BCS theory.

On the other hand, σ for the low T_c ($\sim$ 5 K) compound LaFePO was found to be comparable to that for other high T_c ($\sim$ 30 K) compounds[38]. This means that the LaFePO data point in the T_c–σ plot is far from the Uemura line. Recently, we performed systematic measurements of σ-values for various compounds of LaFeAs$_{1-x}$P$_x$(O,F), and found that with increasing As-content the data point approaches the Uemura-line[39]. This result implies that the coupling strength perhaps originating from electron correlation increases with increasing As-content, as we expect from this study, and as Misawa et al. predicted in their calculations[16,18]. Therefore, in the SC2 phase, the system changes from a weak coupling BCS superconductor to a strong coupling non-BCS one with increasing As-content, while SC1 and SC3 are in the latter regime. Note that the BCS–BEC crossover in multiband superconductors must exhibit properties different from the single band case, as has been theoretically studied for the application to iron-based superconductors[40,41].

Conclusion

The electronic phase diagram was extensively investigated for RFeAs$_{1-x}$(P/Sb)$_x$O$_{1-y}$(F/H)$_y$ (R = La and Nd) over a wide composition range. It was observed that the pnictogen height (h_{Pn}) increases with increasing As/Sb-composition and electron doping, and that h_{Pn} in the Nd-system is larger than that in the La-system. The changes in the superconducting transition temperature (T_c) with composition can be understood in terms of the contribution of the d_{xy} hole Fermi surface (FS) and electron correlation strength, both of which are controlled by h_{Pn}. The apparently-separated two superconducting phases (SC1 and SC3) in the La-system merged with Sb-substitution, suggesting that the origins of these two phases are the same. While FS nesting controlled by band filling plays an important role in the weak coupling BCS superconductivity for the P-rich compositions (SC2 phase), as h_{Pn} increases with increasing As/Sb-content, superconductivity regime switches to strong coupling exotic one with d_{xy} orbital playing an important role (SC1/SC3), which may support the orbital-selective Mott scenario.

Methods

Polycrystalline RFeAs$_{1-x}$(P/Sb)$_x$O$_{1-y}$F$_y$ (R = La and Nd) were synthesized using solid state reaction methods. For R = La, a stoichiometric-ratio mixture of LaAs, LaSb (or LaP), As (or P), Fe$_2$O$_3$, Fe and LaF$_3$ powder was pressed into a pellet in a pure Ar-filled glove box and heated at 1100–1250 °C for 40–60 h in an evacuated silica tube. For R = Nd, a mixture of NdAs, NdP, Fe$_2$O$_3$, Fe and FeF$_2$ powder was used for synthesis. As the solubility limit of fluorine is low ($y < 0.15$–0.20), hydrogen was used to synthesize heavily electron-doped samples ($y = 0.20$ –0.40). H-substituted samples were synthesized under high pressure. Among the above powders, LaF$_3$ and FeF$_2$ were replaced by LaH$_2$ and NdH$_2$ for the La- and Nd-systems, respectively. A mixture of all the chemicals with the appropriate stoichiometric ratio was pressed into a pellet and heated at 1100 °C for 2 h under 4 GPa.

All the samples were characterized using high-resolution X-ray diffraction with beam energy of 11.5 keV and 15 keV at room temperature in BL-8A/8B of Photon Factory in KEK, Japan. The lattice constants, pnictogen (Pn) height from the Fe-plane (h_{Pn}), Pn–Fe–Pn bond angle (α), and Fe–Pn bond distance were calculated from the experimental data by Rietveld analysis[42].

As, P, and Sb concentrations were determined by energy-dispersive X-ray (EDX) spectroscopy. In all samples, the estimated As-, P-, and Sb-concentrations were almost the same as the nominal values. We could not determine the F and H concentrations by EDX, because F and H are light elements.

Magnetic susceptibility measurements were performed using a Magnetic Property Measurement System (MPMS), with an applied field of 10 Oe. Electrical resistivity was measured using a standard four-probe method. Most of the T_c-values presented here were those determined from zero resistivity.

References

1. Kamihara, Y. *et al.* Iron-based layered superconductor: LaOFeP. *J. Am. Chem. Soc.* **128**, 10012 (2006).
2. Kamihara, Y., Watanabe, T., Hirano, M. & Hosono, H. Iron-based layered superconductor La[$O_{1-x}F_x$]FeAs ($x = 0.05$–0.12) with $T_c = 26$ K. *J. Am. Chem. Soc.* **130**, 3296 (2008).
3. Jiang, S. *et al.* Superconductivity up to 30 K in the vicinity of the quantum critical point in $BaFe_2(As_{1-x}P_x)_2$. *J. Phys. Condens. Matter* **21**, 382203 (2009).
4. Kasahara, S. *et al.* Electronic nematicity above the structural and superconducting transition in $BaFe_2(As_{1-x}P_x)_2$. *Nat.* **486**, 382 (2012).
5. Evtushinsky, D. V. *et al.* Propeller-like low temperature Fermi surface of $Ba_{1-x}K_xFe_2As_2$ from magnetotransport and photoemission measurements. *J. Phys. Soc. Jpn.* **80**, 023710 (2011).
6. Malaeb, W. *et al.* Abrupt change in the energy gap of superconducting $Ba_{1-x}K_xFe_2As_2$ single crystals with hole doping. *Phys. Rev. B* **86**, 165117 (2012).
7. Liu, C. *et al.* Importance of the Fermi-surface topology to the superconducting state of the electron-doped pnictide $Ba(Fe_{1-x}Co_x)_2As_2$. *Phys. Rev. B* **84**, 020509 (2011).
8. Borisenko, S. V. *et al.* Superconductivity without nesting in LiFeAs. *Phys. Rev. Lett.* **105**, 067002 (2010).
9. Adachi, T. *et al.* Electronic structure of $Sr_{1-y}Ca_yFe_2(As_{1-x}P_x)2$ ($x = 0.25$, $y = 008$) revealed by angle-resolved photoemission spectroscopy. *J. Phys. Soc. Jpn.* **88**, 084701 (2019).
10. Suzuki, H. *et al.* Strongly three-dimensional electronic structure and Fermi surfaces of $SrFe_2(As_{0.65}P_{0.35})_2$: Comparison with $BaFe_2(As_{1-x}P_x)_2$. *Phys. Rev. B* **89**, 184513 (2014).
11. Charnukha, A. *et al.* Interaction-induced singular Fermi surface in a high-temperature oxypnictide superconductor. *Sci. Rep.* **5**, 10392 (2015).
12. Nishi, I. *et al.* Angle-resolved photoemission spectroscopy study of PrFeAsO0:7: Comparison with LaFePO. *Phys. Rev. B* **84**, 014504 (2011).
13. Takemori, A. *et al.* Change of Fermi surface states related with two different T_c-raising mechanisms in iron pnictide superconductors. *Phys. Rev. B* **98**, 100501 (2018).
14. Yi, M. *et al.* Observation of universal strong orbital-dependent correlation effects in iron chalcogenides. *Nat. Commun.* **6**, 7777 (2015).
15. Maletz, J. *et al.* Photoemission and muon spin relaxation spectroscopy of the iron-based $Rb_{0.77}Fe_{1.61}Se_2$ superconductor: Crucial role of the cigar-shaped Fermi surface. *Phys. Rev. B* **88**, 134501 (2013).
16. Misawa, T., Nakamura, K. & Imada, M. Ab initio evidence for strong correlation associated with Mott proximity in iron-based superconductors. *Phys. Rev. Lett.* **108**, 177007 (2012).
17. de'Medici, L., Giovannetti, G. & Capone, M. Selective Mott physics as a key to iron superconductors. *Phys. Rev. Lett.* **112**, 177001 (2014).
18. Misawa, T. & Imada, M. Superconductivity and its mechanism in an ab initio model for electron-doped LaFeAsO. *Nat. Commun.* **5**, 5738 (2014).
19. Kordyuk, A. A. Electronic band structure of optimal superconductors: From cuprates to ferropnictides and back again. *Low Temp. Phys.* **44**, 477 (2018).
20. Pustovit, Y. V. & Kordyuk, A. A. Metamorphoses of electronic structure of FeSe-based superconductors. *Low Temp. Phys.* **42**, 995 (2016).
21. Bianconi, A. Shape resonances in superstripes. *Nat. Phys.* **9**, 536 (2013).
22. Caivano, R. *et al.* Feshbach resonance and mesoscopic phase separation near a quantum critical point in multiband FeAs-based superconductors. *Supercond. Sci. Technol.* **22**, 014004 (2008).
23. Bussmann-Holder, A. *et al.* The road map toward room-temperature superconductivity: Manipulating different pairing channels in systems composed of multiple electronic components. *Condens. Matter* **2**, 24 (2017).
24. Lee, C.-H. *et al.* Effect of structural parameters on superconductivity in fluorine-free $LnFeAsO_{1-y}$ (Ln = La; Nd). *J. Phys. Soc. Jpn.* **77**, 083704 (2008).
25. Mizuguchi, Y. *et al.* Anion height dependence of T_c for the Fe-based superconductor. *Supercond. Sci. Technol.* **23**, 054013 (2010).
26. Kuroki, K., Usui, H., Onari, S., Arita, R. & Aoki, H. Pnictogen height as a possible switch between high-T_c nodeless and low-T_c nodal pairings in the iron-based superconductors. *Phys. Rev. B* **79**, 224511 (2009).
27. Miyasaka, S. *et al.* Two fermi surface states and two T_c-rising mechanisms revealed by transport properties in $RFeP_{1-x}As_xO_{0.9}F_{0.1}$ (R = La, Pr, and Nd). *J. Phys. Soc. Jpn.* **82**, 124706 (2013).
28. Lai, K. T. *et al.* Evolution of the phase diagram of $LaFeP_{1-x}As_xO_{1-y}F_y$ ($y = 0$–0.1). *Phys. Rev. B* **90**, 064504 (2014).
29. Miyasaka, S. *et al.* Three superconducting phases with different categories of pairing in hole- and electron-doped $LaFeAs_{1-x}P_xO$. *Phys. Rev. B* **95**, 214515 (2017).
30. Ricci, A. *et al.* The microstrain-doping phase diagram of the iron pnictides: Heterostructures at atomic limit. *J. Supercond. Nov. Magn.* **22**, 589 (2009).
31. Gurvitch, M. Universal disorder-induced transition in the resistivity behavior of strongly coupled metals. *Phys. Rev. Lett.* **56**, 647 (1986).
32. Tin, Z. H. Doctor Thesis (Osaka University, 2020).
33. Usui, H., Suzuki, K. & Kuroki, K. Origin of the non-monotonic variance of T_c in the 1111 iron based superconductors with isovalent doping. *Sci. Rep.* **5**, 11399 (2015).
34. Mazin, I. I., Singh, D. J., Johannes, M. D. & Du, M. H. Unconventional superconductivity with a sign reversal in the order parameter of $LaFeAsO_{1-x}F_x$. *Phys. Rev. Lett.* **101**, 057003 (2008).
35. Kuroki, K. *et al.* Unconventional pairing originating from the disconnected Fermi surfaces of superconducting $LaFeAsO_{1-x}F_x$. *Phys. Rev. Lett.* **101**, 087004 (2008).
36. Kontani, H. & Onari, S. Orbital-fluctuation-mediated superconductivity in iron pnictides: Analysis of the five-orbital Hubbard–Holstein model. *Phys. Rev. Lett.* **104**, 157001 (2010).
37. Uemura, Y. J. *et al.* Basic similarities among cuprate, bismuthate, organic, Chevrel-phase, and heavy-fermion superconductors shown by penetration-depth measurements. *Phys. Rev. Lett.* **66**, 2665 (1991).
38. Carlo, J. P. *et al.* Static magnetic order and superfluid density of $RFeAs(O, F)$ (R = La, Nd, Ce) and LaFePO studied by Muon spin relaxation: Unusual SIMILARITIES WITH THE BEHAVIOR OF CUPRATE superconductors. *Phys. Rev. Lett.* **102**, 087001 (2009).
39. Miyasaka, S. *et al.* In preparation.
40. Guidini, A. & Perali, A. Band-edge BCS–BEC crossover in a two-band superconductor: Physical properties and detection parameters. *Supercond. Sci. Technol.* **27**, 124002 (2014).
41. Tajima, H., Yerin, Y., Pieri, P. & Perali, A. Mechanisms of screening or enhancing the pseudogap throughout the two-band Bardeen–Cooper–Schrieffer to Bose–Einstein condensate crossover. *Phys. Rev. B* **102**, 220504 (2020).
42. Izumi, F. & Momma, K. Three-dimensional visualization in powder diffraction. *Solid State Phenom.* **130**, 15 (2007).

Acknowledgements

Author contributions

S.M. proposed the study and played a coordinating role. T.K., H.T., T.Y., M.U., A.T., and K.T.L. synthesized the samples and measured them. T.K., S.M., and S.T. discussed the results, and wrote the manuscript.

Competing interests

The authors declare no competing interests.

Additional information

Supplementary information The online version contains supplementary material available at https://doi.org/10.1038/s41598-021-89231-2.

Correspondence and requests for materials should be addressed to S.M.

Reprints and permissions information is available at www.nature.com/reprints.

Publisher's note Springer Nature remains neutral with regard to jurisdictional claims in published maps and institutional affiliations.